

**POTENTIAL NEURAMINIDASE INHIBITORS
VIA VIRTUAL SCREENING, KINETIC STUDIES,
AND ADME PREDICTIONS**

RINA FAJRI NUWARDA

UNIVERSITI SAINS MALAYSIA

2015

**POTENTIAL NEURAMINIDASE INHIBITORS
VIA VIRTUAL SCREENING, KINETIC STUDIES,
AND ADME PREDICTIONS**

by

RINA FAJRI NUWARDA

**Thesis submitted in fulfillment of the requirements
for the Degree of Master of Science**

October 2015

ACKNOWLEDGEMENTS

In the name of Allah, the Most Gracious, the Most Merciful.

All praise is due Allah, for giving me strength and opportunity to do this work and for putting so many good people in my way. May Allah's peace and blessing be upon Prophet Muhammad (Peace be upon him), whose way of life has been a continuous model for mankind.

First and foremost, I would like to express my sincere gratitude and deep appreciation to my supervisor, Prof. Habibah Abdul Wahab, who gave me the opportunity to work in this research group, her continuous support, motivation, and guidance have made this thesis possible. I am also very grateful to my co-supervisor Assoc. Prof. Dr. Tan Mei Lan for her time and untiring assistance she has kindly spent to guide my research, without which it would have been impossible to complete my thesis.

My heartfelt thanks to Yusuf and Maywan, for being really supportive friends all the time, and also to my senior Safri, for his help, encouragement and valuable discussions. Many thanks to my fellow lab mates in the Pharmaceutical Design and Simulation Laboratory (PhDS) Universiti Sains Malaysia and also to the coolest lab companions ever: Asyraf, Yea Lu, Yi Fan, Yanti, Anis, and Yoong Min in the Lead Optimization Division Institut Farmasetikal dan Nutrasetikal Malaysia (IPHARM). This work could not have been completed without their help and contributions.

Furthermore, I'd like to thank Nadia, Izzati, and Fatemeh for their wonderful friendship since the very first time I started my study. Special thanks to my friends in the Indonesian Student Association (PPI) Universiti Sains Malaysia, and also my international friends Bija, Hamza, Nadirah, Mahmoud, Bilal, Abdullah, and Hidayu who have been the best family during my stay in Penang. Thank you for all the moments we spent together, for the friendships and comforting words through rough times in our study. My sincere thank also goes to my big family and best friends in Indonesia for always supporting me in any way possible.

Last but not least, no words are ever sufficient to express my everlasting gratitude, appreciation and thanks to my beloved, wonderful parents for their constant supports, prayers and inspiration. My sister Widya, for always being such an understanding and uplifting one, there's really no better friend than a sister. My heartfelt love and thanks to them for always believing in me and helping me in every way while I work to achieve my dreams.

Al-hamdu lillahi rabbil 'alamin.

TABLE OF CONTENTS

	Page
ACKNOWLEDGEMENT	ii
TABLE OF CONTENTS	iv
LIST OF TABLES	x
LIST OF FIGURES	xi
LIST OF SCHEMES	xvii
LIST OF SYMBOLS AND ABBREVIATIONS	xviii
LIST OF PUBLICATIONS AND CONFERENCES	xx
ABSTRAK	xxi
ABSTRACT	xxiii
CHAPTER 1 – INTRODUCTION	1
1.1. Statement of the Problem	1
1.2. The Influenza	4
1.2.1. Epidemics and Pandemics	4
1.2.2. The Influenza Virus	7
1.2.3. Influenza Virus Life Cycle	8
1.2.4. Influenza Virus Neuraminidase	10
1.2.4.1. Structure of Neuraminidase	10
1.2.4.2. The Substrate and the Active site of Neuraminidase	12
1.2.4.3. Neuraminidase Inhibitor	16
1.3. Computational Methods for Drug Discovery	18
1.4. Enzyme Kinetics	23

	Page
1.4.1. Maximum Rate of Metabolism (V_{max}) and Michaelis Constant (K_m)	23
1.4.2. Inhibition Constant (K_i)	26
1.5. Absorption, Distribution, Metabolism, and Excretion (ADME) of Compounds	29
1.5.1. Overview	29
1.5.2. Drug Absorption	30
1.5.3. Drug Distribution	32
1.5.4. Drug Metabolism	33
1.5.5. Drug Excretion	34
CHAPTER 2 – MATERIALS AND METHODS	36
2.1. Materials and Reagents	36
2.2. Instruments	36
2.3. Overview of the Methodology	38
2.4. Automated Flexible Ligand Docking Of NCI Compound Database	40
2.4.1. Software	41
2.4.2. Preparation of Target Macromolecule (3TI6)	41
2.4.3. Positive Control Docking	42
2.3.3.1. Preparation of Ligand (Oseltamivir/NCI)	42
2.3.3.2. Creating Grid Parameter File	42
2.3.3.3. Creating Docking Parameter File	43
2.4.4. Virtual Screening of NCI Database	43
2.5. Development of Neuraminidase Inhibition Assay using Alphascreen Technology	44
2.5.1. Biotinylation of lpha-1-acid glycoprotein (AGP)	44

	Page
2.5.1.1. Buffer Exchange	44
2.5.1.2. Determination of AGP Concentration Using BCA (Bicinchoninic Acid Assay) Protein Assay Kit	45
2.5.1.3. Preparation of ChromaLink Biotin Reagent Water Soluble	46
2.5.1.4. Biotinylation Reaction	46
2.5.1.5. Desalting Procedure	47
2.5.1.6. Quantification of Biotin Incorporation in Biotinylated AGP	47
2.5.1.7. TruHits Detection of Biotinylated AGP	48
2.5.2. Protein-protein Interaction Experiments: Biotinylated AGP and Lectin WGA Acceptor Beads Binding Partner	51
2.5.2.1. Biotinylated AGP and Lectin WGA Binding Experiment	51
2.5.2.2. Buffer Optimization	51
2.5.2.3. Biotinylated AGP and Lectin WGA Binding Experiment in the Presence of NA	52
2.5.2.4. Optimization of NA and biotinylated AGP via Cross Titration Experiment	53
2.5.3. Validation of Assay Protocol with Oseltamivir Carboxylate ...	54
2.6. Fluorometric neuraminidase assay using MUNANA as substrate	56
2.6.1. Preparation of Stock Solution	57
2.6.2. Preparation of the Working Solution	58
2.6.3. Preparation of Substrate and Enzyme	58
2.6.4. Neuraminidase Optimal Activity Assay	58
2.6.5. Validation of MUNANA assay using oseltamivir carboxylate and 2-deoxy-2,3-didehydro-N-acetylneuraminic acid (DANA)	59
2.6.6. Neuraminidase inhibition assay for <i>in silico</i> hits compounds ..	60

	Page
2.6.6.1. Preparation of <i>in silico</i> Hits Compounds	60
2.6.6.2. Inhibition Assay of <i>in silico</i> Hits Compounds	60
2.6.7. Neuraminidase Kinetic Assay	62
2.6.7.1. Determination of V_{max} and K_m for MUNANA	62
2.6.7.2. Determination of K_i for Neuraminidase Inhibitor ...	62
2.7 In <i>silico</i> ADME Prediction of top NCI Compounds	63
2.7.1. Software	63
2.7.2. Methods	64
CHAPTER 3 – RESULTS AND DISCUSSIONS	65
3.1. Automated Flexible Ligand Docking of NCI Compound Database	65
3.1.1. Control Docking with Oseltamivir	65
3.1.2. Virtual Screening Results	67
3.2. Development of Neuraminidase Inhibition Assay using AlphaScreen technology	86
3.2.1. Biotinylation of alpha-1-acid glycoprotein (AGP)	89
3.2.2. Protein-protein Interaction Experiments: Biotinylated AGP and Lectin WGA Acceptor Beads Binding Partner	93
3.2.2.1. Biotinylated AGP - Lectin WGA Binding Experiment	93
3.2.2.2. Buffer Optimization	95
3.2.2.3. Biotinylated AGP and Lectin WGA Binding Experiment in the Presence of NA	98
3.2.2.4. Biotinylated AGP-Lectin WGA Cross Titration Experiment	99
3.2.3 Validation of Assay Protocol with OTV as Known Inhibitor	102
3.3. Fluorometric Neuraminidase Assay Using MUNANA as Substrate ...	105

	Page
3.3.1. NA Optimal Activity Assay	106
3.3.2. Validation of MUNANA Assay Using Oseltamivir carboxylate and 2-deoxy-2,3-didehydro-N-acetylneuraminic acid (DANA)	107
3.3.3. Neuraminidase Inhibition Assay For 40 <i>In Silico</i> Hits Compounds	108
3.3.4. Neuraminidase Kinetic Assay	119
3.3.4.1. Determination of V_{max} and K_m for MUNANA	120
3.3.4.2. Inhibition Constant for Oseltamivir Carboxylate and DANA as Known NA Inhibitor	121
3.3.4.3. Inhibition Constant for Top 4 <i>in vitro</i> Compounds .	123
3.4. Absorption, Distribution, Metabolism, and Excretion of NCI Top Compounds	125
3.4.1. Assessment of Drug-likeness Properties	126
3.4.2. Assessment of Pharmacokinetic Properties	129
3.4.2.1. Degree of ionization (pKa)	129
3.4.2.2. Topological Polar Surface Area (TPSA)	131
3.4.2.3. Fraction Absorbed (%F)	132
3.4.2.4. Volume Distribution (Vd)	132
3.4.2.5. Plasma protein binding (%PPB)	133
3.4.2.6. Cytochrome (CYP) P450 Inhibitors and Substrate Probability)	133
CHAPTER 4 – CONCLUSION	137
4.1. Objective Accomplishment	137
4.2. Recommendation for Future Studies	140

	Page
REFERENCES	141
APPENDICES	151

LIST OF TABLES

		Page
Table 2.1	Materials and Reagents	37
Table 2.2	Parameters of molecular docking for virtual screening of NCI database	43
Table 2.3	The composition of well and expected signal generated in the biotin AGP-Lectin WGA experiments	56
Table 2.4	Composition of each well: (●) inhibitor; (●) blank; and (●) positive control.	62
Table 3.1	Two-dimensional structure of compounds from virtual screening results, consists of 39 compounds and 1 compound as the top rank and the lowest rank of FEB, respectively.	68
Table 3.2	Amino acid residue involved in the hydrogen bond and pi-pi interactions between ligand and NA of the selected compounds.	84
Table 3.3	Free energy of binding and % inhibition of selected NCI compounds from virtual screening experiments.	109
Table 3.4	Assessment of drug-likeness properties based on Lipinski's Rule-of-Five.	128
Table 3.5	Assessment of pharmacokinetic properties	130
Table 3.6	Cytochrome (CYP) P450 inhibitors and substrate probability for top 4 compounds	135

LIST OF FIGURES

		Page
Figure 1.1	Influenza virus can change in two different way. Antigenic drift is small changes in the virus that produce new virus strains that may not be recognized by the body's immune system while antigenic shift is an abrupt, major change resulting new hemagglutinin and/or new hemagglutinin and neuraminidase proteins in influenza viruses	5
Figure 1.2	Diagram of Influenza A virus. On the outside virus particles, 3 viral proteins: haemagglutinin (HA, trimers), neuraminidase (NA) (tetramers) and M2 (tetramers that make up ion-channels) are exposed	8
Figure 1.3	Influenza virus replication cycle (Gubareva et al., 2000)	10
Figure 1.4	Three dimensional structure of an N2 neuraminidase tetramer in complex with sialic acids (PDB ID 2BAT) (Varghese et al., 1992)	11
Figure 1.5	a. The two most common sialic acids are <i>N</i> -acetyl neuraminic acid (Neu5Ac) and <i>N</i> -glycolylneuraminic acid (Neu5Gc). b. Sialic acids are attached to carbohydrate chains on glycoproteins and glycolipids via different glycosidic linkages. The most common linkage types are α 2, 3-linkage to a galactose residue, α 2,6-linkage to a galactose moiety or to an <i>N</i> -acetylgalactosamine moiety, and α 2,8-linkage to another sialic acid moiety on a glycan (Stencel-Baerenwald et al., 2014)	13
Figure 1.6	Neuraminidase active site consists of functional amino acid residues Arg118, Asp151, Arg152, Arg224, Glu 276, Arg292, Arg371, and Tyr406, which are in direct contact with sialic acid, and structural amino acids residue Glu119, Arg156, Trp178, Ser179, Asp (or Asn in N7 and N9)198, Ile222, Glu227, Glu277, Asp293, and Glu42. (Protein Data Bank ID: 2BAT www.rcsb.org)	15
Figure 1.7	Mechanism of Action of Neuraminidase Inhibitors. Panel A shows the action of neuraminidase in the continued replication of virions in influenza infection. The replication is blocked by neuraminidase inhibitors (Panel B), which prevent from being release from the surface of infected cells.	16

	Page
Figure 1.8 Neuraminidase crystal structure in complex with zanamivir (PDB ID: 3B7E) (Xu et al., 2008)	18
Figure 1.9. Mechanism of ligand interactions in the receptor binding site	22
Figure 1.10 Velocity of product formation or substrate disappearance is defined as the change in product concentration per unit time. Velocity is the slope of a plot o product concentration against time	24
Figure 1.11 Plot of Michaelis-Menten equation, reaction velocity as a function of substrate concentration, where the substrate concentration affects the velocity of reaction. The significance of kinetic parameters Vmax and Km are depicted	25
Figure 1.12 Determination of Km with Lineweaver-Burk Plot	26
Figure 1.13 Lineweaver-Burk Plot for competitive, uncompetitive, and noncompetitive enzyme inhibition	27
Figure 1.14 Determination of Inhibition constant (Ki) - Dixon Plot for competitive inhibition	28
Figure 1.15 Determination of Inhibition constant (Ki) - Dixon Plot for noncompetitive inhibition.	29
Figure 2.1 Overview of the methodology	39
Figure 2.2 Flow chart of molecular docking and virtual screening experiments	40
Figure 2.3 Flow chart of development of neuraminidase inhibition assay AlphaScreen™ technology	44
Figure 2.4 ChromaLink Biotin Protein Labeling Calculator	46
Figure 2.5 BCA ChromaLink Biotin MSR Calculator to determine biotin incorporation into protein	48
Figure 2.6 Biotinylation of AGP illustration and summarized protocol	50
Figure 2.7 Summarize protocol and illustration of Biotin AGP-Lectin WGA binding experiments	54
Figure 2.8 Flow chart of MUNANA assay (inhibition and kinetic assay) and <i>in silico</i> ADME prediction.	57

	Page
Figure 2.9	Illustration of the 96-well microplate for NA optimal activity assay. Each well contains 50 μ L NA and 50 μ L MUNANA. Wells with red colors represent serial dilution of NA, while wells with green colors represent negative control (without NA) and yellow colors represent blank (buffer) 59
Figure 2.10	Illustration of the 96-well microplate for inhibition assay 61
Figure 2.11	Illustration of the 96-well microplate for kinetic assay. Each well contains 25 μ L of inhibitors, 25 μ L NA, and 50 μ L MUNANA 63
Figure 3.1	Cluster analysis of docking result of oseltamivir as control ligand. Histogram showed that there are four clusters resulted in the docking simulation. The lowest binding energy with value -9.75 kcal was found in the largest cluster 66
Figure 3.2	The superposition of the initial pose (green color) and the control docking pose (blue color) of oseltamivir (PDB ID 3TI6). RMSD value obtained was 0.97 Å 67
Figure 3.3	Overlay of NSC 5069 structure (green carbon color) with OTV (turquoise carbon color) and their binding to neuraminidase active site in 3TI6 crystal structure. Dashed lines represented the H-bonds between these compounds and important amino acid residues of 3TI6 82
Figure 3.4	Two dimensional (2D) diagram of NSC 293778 showing Pi interactions (orange lines) between ligand and amino acid residues in NA binding site. Blue dots and blue circles are the part of compounds or amino acid residues which are exposed to solvent 83
Figure 3.5	Alpha-1-acid Glycoprotein structure, sialic acid structure was presented in green color (PDB ID: 3APU) 88
Figure 3.6	Biotinylation of AGP allows the protein to interact with streptavidin-coated donor beads 91
Figure 3.7	TruHits signal inhibition by increasing concentration of AGP. AGP final concentration ranging from 0.3 nM to 300 nM were used 92
Figure 3.8	A bell-shaped curve obtain from Biotin AGP titration experiment 94
Figure 3.9	Competition assay using unlabeled AGP..... 95

	Page
Figure 3.10 Optimization with three kinds of buffer: (1) PBS (2) MES (3) HEPES	96
Figure 3.11 Buffer optimization: Addition of detergent Tween-20 and BSA	97
Figure 3.12 Effect of NA to the binding of Biotin AGP- Lectin WGA. Increasing concentration of NA resulted in signal decrease	98
Figure 3.13 Typical bell-shaped curve obtained from Biotin AGP and Lectin WGA cross titration experiments	100
Figure 3.14 Biotin AGP- Lectin WGA binding partner in the development of NA inhibition assay using AlphaScreen technology. The presence of NA interrupted the binding and generate signal loss.	101
Figure 3.15 Validation of AlphaScreen assay using oseltamivir (1) with 100nM NA; (2) with 10nM NA; (2) various incubation time ...	102
Figure 3.16 Schematic representation of the hydrolysis of 4-MUNANA catalysed by neuraminidase. The reaction product: 4-methylumbelliferone (4-MU) is quantified fluorimetrically by using an excitation wavelength of 355 nm and the emission at 460 nm.....	105
Figure 3.17 H1N1 NA optimum activity (at concentration 0.039 U/ml). Experiment was done in triplicate	106
Figure 3.18 Inhibition activity of oseltamivir carboxylate against H1N1 NA (3 replicates)	107
Figure 3.19 Inhibition activity of DANA against H1N1 NA (3 replicates) ...	108
Figure 3.20 Percentage of enzyme activity of NSC 5069 against H1N1 NA (3 replicates)	110
Figure 3.21 Percentage of enzyme activity of NSC 83318 against H1N1 NA (3 replicates)	111
Figure 3.22 Percentage of enzyme activity of NSC 156563 against H1N1 NA (3 replicates)	111
Figure 3.23 Percentage of enzyme activity of NSC 134137 against H1N1 NA (3 replicates)	112
Figure 3.24 24 Percentage of enzyme activity of NSC 148304 against NA. (3 replicates)	112

	Page	
Figure 3.25	2D diagram (a) and 3D docking pose (b) of NSC 5069. In the 2D diagram hydrogen bonds are presented in dashed lines and Pi interactions are presented in orange lines, meanwhile blue dots and blue circles are the part of compounds or amino acid residues which are exposed to solvent. Functional groups of these compounds interact via hydrogen bond with important residues of NA, namely Arg118, Arg292, Arg371, Tyr406, and Asp151	113
Figure 3.26	2D diagram (a) and 3D docking pose (b) of NSC 83318. In the 2D diagram hydrogen bonds are presented in dashed lines and Pi interactions are presented in orange lines, meanwhile blue dots and blue circles are the part of compounds or amino acid residues which are exposed to solvent. Functional groups of these compounds interact via hydrogen bond with important residues of NA, namely Arg118, Arg292, Arg371 and Tyr406..	114
Figure 3.27	2D diagram (a) and 3D docking pose (a) of NSC 156563. In the 2D diagram hydrogen bonds are presented in dashed lines and Pi interactions are presented in orange lines, meanwhile blue dots and blue circles are the part of compounds or amino acid residues which are exposed to solvent. Functional groups of these compounds interact via hydrogen bond with important residues of NA, namely Arg118, Arg292, Arg371 and Tyr406..	116
Figure 3.28	2D diagram (a) and 3D docking pose (b) of NSC 134137. In the 2D diagram hydrogen bonds are presented in dashed lines and Pi interactions are presented in orange lines, meanwhile blue dots and blue circles are the part of compounds or amino acid residues which are exposed to solvent. Functional groups of these compounds interact via hydrogen bond with important residues of NA, namely Arg118, Arg292, Arg371 and Tyr406..	117
Figure 3.29	2D diagram (a) and 3D docking pose (b) of NSC 148304 showing few hydrogen bonds between compound and Arg224, Arg276, and Glu227. In the 2D diagram hydrogen bonds are presented in dashed lines and Pi interactions are presented in orange lines, meanwhile blue dots and blue circles are the part of compounds or amino acid residues which are exposed to solvent ..	118
Figure 3.30	Michaelis-Menten plot from determination of Michaelis-Menten constant (K_m) for MUNANA and maximum reaction velocity (V_{max})	120

	Page
Figure 3.31 Lineweaver-Burk Plot for determining K_m and V_{max}	121
Figure 3.32 Dixon plot for Oseltamivir Carboxylate as NA inhibitor. [I] is the concentration of inhibitor. K_i value: 1.70 nM. Type of inhibition: competitive inhibition (see Figure 1.14 page 29)	122
Figure 3.33 Lineweaver-Burk plot for DANA as NA inhibitor. [I] is the concentration of inhibitor. K_i value: 9.93 μ M. Type of inhibition: competitive inhibition (see Figure 1.14 page 29)	122
Figure 3.34 Dixon plot for NSC 5069. [I] is the concentration of inhibitor. Type of inhibition: competitive inhibition. K_i value: 100.26 μ M	123
Figure 3.35 Dixon plot for NSC 83318. [I] is the concentration of inhibitor. Type of inhibition: competitive inhibition. K_i value: 204.13 μ M	124
Figure 3.36 Dixon plot for NSC 156563. [I] is the concentration of inhibitor. Type of inhibition: competitive inhibition. K_i value: 202.9 μ M	124
Figure 3.37 Dixon plot for NSC 134137. [I] is the concentration of inhibitor. Type of inhibition: competitive inhibition. K_i value: 197.75 μ M	125

LIST OF SCHEMES

	Page	
Scheme 1.1	Reaction steps and corresponding intermediates of catalytic pathway of neuraminidase	15
Scheme 1.2	A typical docking workflow. This flowchart shows the key steps common to all docking protocols. The 3D structures for the target macromolecule and the small molecule must first be chosen, and then each structure must be prepared in accordance with the requirements of the docking method being used. Following the docking, the results must be analyzed, selecting the binding modes with the best scores.	21
Scheme 1.3	Drug disposition process which is divided into four parts: Absorption, distribution, metabolism, and excretion	30

LIST OF SYMBOLS AND ABBREVIATIONS

% F	% Fraction absorbed
3D	Three-dimensional
Å	Angstrom
ACD	Advance Chemistry Development
ADME	Absorption, Distribution, Metabolism, and Excretion
ADT	AutoDock Tools
AGP	alpha 1-acid glycoprotein
Arg	Arginine
Asn	Asparagine
Asp	Aspartic acid
BBB	Blood Brain Barrier
BCA	Bicinchoninic acid
BSA	bovine serum albumin
Camp	cyclic-adenosine monophosphate
CDC	Centre of Disease Control and Prevention
Cl _{int}	Intrinsic clearance
CNS	Central Nervous System
CYP	Cytochrome P450
DANA	2,3-didehydro-2-deoxy-N-acetylneuraminic acid
DMSO	Dimethyl sulfoxide
DNA	Deoxyribonucleic acid
E	Enzyme
EC	Enzyme commission
FDA	Food and Drug Administration
FEB	Free Energy of Binding
GA	Genetic Algorithm
Glu	Glutamic acid
GPCR	G protein-coupled receptor
GSH	Glutathione
GUI	Graphic User Interface
HA	Hemagglutinin
HBA	hydrogen bond acceptor
HBD	hydrogen bond donor
HEPES	(4-(2-hydroxyethyl)-1-piperazineethanesulfonic acid)
HTS	High-throughput screening
Ile	Isoleucine
IP3	Inositol trisphosphate
K _i	Inhibition constant
K _m	Michaelis constant
LGA	Lamarckian Genetic Algorithm
Log P	Partition coefficient
M1	Matrix protein 1
M2	Matrix protein 2
MC	Monte Carlo
MES	2-(N-morpholino)ethanesulfonic acid
MGL	Molecular Graphic Laboratory

MRP2	Multidrug Resistance-associate Protein 2
MUNANA	2'-(4-Methylumbelliferyl)- α -D-N-acetylneuraminic acid
MW	molecular weight
NA	Neuraminidase
NANA	N-Acetylneuraminic acid
NCI	National Cancer Institute
Neu5Ac	N-Acetylneuraminic acid
Neu5Ac	N-acetylneuraminic acids
Neu5Gc	N-Glycolylneuraminic acid
Neu5Gc	N-glycolylneuraminic acids
NH ₂	Amino
NP	Nucleoprotein
NS	Non-structural
-OH	Hydroxyl group
P	Product
PA	Polymerase acidic protein
PB	Polymerase basic protein
PBS	Phosphate buffered saline
PDB	Protein data bank
P-gp	P-glycoprotein
pK _a	Acid dissociation constant
PMV	Phyton Molecular Viewer
QSAR	Quantitative Structure Activity Relationship
RdRp	RNA-dependent RNA polymerase
RNA	Ribonucleic acid
S	Substrate
SA	Sialic acid
Ser	Serine
-SH	sulfohydryl group
Trp	Tryptophan
Tyr	Tyrosine
UDP	Uridine5'-diphospho-glucuronosyltransferase (UDP-glucuronosyltransferase
UGT	Uridine 5'-diphospho-glucuronosyltransferase
V _{max}	Maximum velocity
V _o	Initial velocity
vRNP	Viral ribonucleoprotein
WHO	World Health Organization
α	alpha
β	beta

LIST OF PUBLICATIONS AND CONFERENCES

Conference Proceeding / Book of Abstract / Oral Presentation / Poster Presentation

NUWARDA, R. F., WAHAB, H. A., TAN, M. L. 2011. Development of a High-Throughput Screening (HTS) Assay for Influenza Neuraminidase H1N1 Using AlphaScreen™ Technology. The 2nd International Seminar on Chemistry, Bandung – Indonesia, 24-25 November 2011

**PERENCAT NEURAMINIDASE BERPOTENSI MELALUI SARINGAN
MAYA, KAJIAN KINETIK, DAN JANGKAAN ADME**

ABSTRAK

Aktiviti neuraminidase (NA) memainkan peranan yang penting dalam jangkitan oleh virus influenza dengan memudahkan pelepasan virion yang baru ditubuhkan daripada reseptor sel tuan rumah dan menggalakkan jangkitan kepada sel-sel atau organ-organ lain. Disebabkan kemunculan rintangan virus terhadap perencat NA sedia ada, penemuan perencat NA baru amat diperlukan. Dalam kajian ini, pemeriksaan maya berdasarkan pendokan sebatian-sebatian daripada pangkalan data NCI untuk memilih dengan pantas hit *in silico* bagi menjadi potensi perencat NA telah dijalankan. Satu kaedah *in vitro* baru telah dicuba untuk membangunkan perencatan asai NA dengan menggunakan teknologi AlphaScreenTM dengan Alpha-1-Asid Glikoprotein sebagai substrat. Malangnya, usaha ini tidak berjaya mungkin disebabkan pemisahan tidak spesifik asid sialik oleh NA. Selepas itu, asai MUNANA tradisional telah dijalankan untuk menyiasat aktiviti perencatan dan parameter kinetik sebatian perencat. Akhir sekali, sebatian-sebatian terpilih dikaji untuk ciri farmakokinetik *in silico* mereka. Dari pangkalan data NCI, 1541 sebatian telah berjaya disaring untuk mendapatkan 40 kompaun hit *in silico* diikuti oleh asai MUNANA untuk menentukan IC₅₀ mereka. Sepuluh daripada mereka menunjukkan lebih daripada 50% perencatan terhadap NA dan empat sebatian iaitu NSC 5069, NSC 83318, NSC 156563, dan NSC 134137 didapati mempunyai nilai IC₅₀ sebanyak masing-masing 216 µM, 320 µM, 571 µM dan 673 µM. Kajian kinetik menunjukkan nilai K_m untuk MUNANA ialah 36.44 µM dan V_{max} bagi tindak balas enzim ialah 551.25 RFU / min. Daripada plot Dixon, semua sebatian mempunyai daya saing dengan nilai K_i untuk NSC 5069, NSC

83318, NSC 156563 dan NSC 134137 masing-masing ialah 100.26 μM , 204.13 μM , 202.9 μM , 197.75 μM . Penilaian ciri-ciri kesamaan-dadah meramalkan sifat-sifat fizikokimia seperti berat molekul, Log P, bilangan ikatan hidrogen penderma dan penerima memenuhi Peraturan Lima Lipinski. Hasil nilai pK_a menunjukkan bahawa sebatian berasid lemah dan cenderung untuk diserap dalam usus (NSC 5069 dengan nilai pK_a 4.1, dan NSC 83318 dengan nilai pK_a 6.3), dan kompaun berasid lebih kuat untuk diserap dalam perut (NSC 156563 dan NSC 134137 dengan nilai pK_a 2.7). Pengiraan *in silico* TPSA menunjukkan bahawa NSC 83318 dan NSC 156563 memenuhi kriteria Lipinski dengan mempunyai nilai TPSA kurang daripada 140 A^2 , manakala NSC 5069 dan NSC 134137 telah diramalkan untuk mempunyai penyerapan lemah kerana nilai TPSA mereka adalah lebih daripada had yang boleh diterima 140 A^2 . Berdasarkan peratusan fraksi diserap, NSC 5069 dan NSC 83318 telah dianggap mempunyai fraksi tinggi untuk penyerapan. Manakala dua sebatian, NSC 156563 dan NSC 134137 telah mempunyai fraksi rendah untuk penyerapan. Dalam meramalkan isipadu pendedaran, hasil menunjukkan bahawa isipadu pendedaran NSC 5069, NSC 83318, NSC 156563, NSC 134137 masing-masing adalah 0.86 L/kg, 0.7 L/kg, 0.13 L/kg dan 0.12 L/kg. NSC 83318, NSC 156563, dan NSC 134137 mempunyai %PPB lebih daripada 90% yang bermakna bahawa hampir semua sebatian ditadbir boleh terikat kepada protein plasma dalam badan, manakala NSC 5069 mempunyai %PPB 57%, menunjukkan bahawa 57% daripada kompaun adalah terikat kepada protein plasma. Akhir sekali, empat sebatian utama tidak menunjukkan kebarangkalian sebagai substrat atau perencat bagi kebanyakan isoform CYP, kecuali NSC 83318 yang menunjukkan kebarangkalian yang tinggi untuk bertindak sebagai CYP 1A2 dengan nilai 0.84.

POTENTIAL NEURAMINIDASE INHIBITORS VIA VIRTUAL SCREENING, KINETIC STUDIES, AND ADME PREDICTIONS

ABSTRACT

Neuraminidase (NA) activity plays an important role in the infection by influenza viruses by facilitating the release of the newly formed virions from the host cell receptor and promotes its infection to other cells or organs. With the emergence of viral resistance towards the existing NA inhibitors, the discovery of new NA inhibitors is urgently needed. In this work, docking-based virtual screening of large compounds from NCI database to rapidly select *in silico* hits to be potential NA inhibitors was carried out. A new *in vitro* method has been attempted to be developed for NA inhibition assay by utilizing AlphaScreen™ technology with Alpha-1-Acid glycoprotein as a substrate. Unfortunately, this effort was unsuccessful probably due to the non-specific cleavage of sialic acid by NA. Subsequently, a traditional MUNANA assay was performed to investigate the inhibitory activities and kinetic parameters of the inhibitor compounds. Finally, the selected compounds were studied for their pharmacokinetic properties *in silico*. From the NCI database, 1541 compounds have been successfully screened and 40 *in silico* hits compounds were obtained, and assayed to determine their IC₅₀s. Ten of them demonstrated over 50% inhibition against NA and four compounds namely NSC 5069, NSC 83318, NSC 156563, and NSC 134137 were found having IC₅₀ values of 216 μM, 320 μM, 571 μM and 673 μM, respectively. The kinetic studies showed K_m value for MUNANA was 36.44 μM and V_{max} for the enzymatic reaction was 551.25 RFU/min. From the Dixon plot, these four compounds appeared to competitively inhibit the neuraminidase with K_i values for NSC 5069, NSC 83318, NSC 156563, and NSC 134137 were 100.26,

204.13, 202.90, and 197.75 μM , respectively. Drug-likeness properties assessment predicting the physicochemical properties such as molecular weight, Log P, number of hydrogen bond donor and acceptor fulfilled Lipinski's Rule of Five. The results of pKa value showed that the compounds are weakly acidic and tend to be absorbed in the intestine (NSC 5069 with pKa value 4.1, NSC 83318 with pKa value 6.3 and), and stronger acidic compound to be absorbed in the gastrik (NSC 156563 and NSC 134137 with pKa value 2.7). *In silico* calculations of TPSA showed that NSC 83318 and NSC 156563 fulfill Lipinski's criteria of having TPSA value less than 140 \AA^2 , while NSC 5069 and NSC 134137 were predicted to have poor permeation since their TPSA values are more than the acceptable upper limit of 140 \AA^2 . Based on the fraction's absorbed percentage, NSC 5069 and NSC 83318 were considered to have high fraction for the absorption. While the other two compounds, NSC 156563 and NSC 134137 had low fraction for the absorption. In predicting volume distribution, the results showed that the volume distribution of NSC 5069, NSC 83318, NSC 156563, NSC 134137 were 0.86 L/kg, 0.7 L/kg, 0.13 L/kg and 0.12 L/kg, respectively. NSC 83318, NSC 156563, and NSC 134137 have %PPB more than 90% which means that almost all the compounds administered may be bound to the plasma protein in the body, whereas NSC 5069 has %PPB 57%, indicating that 57% of the compound is bound to the plasma proteins. Lastly, the four top compounds showed no probability as substrates or inhibitors for almost all CYP isoforms, except for NSC 83318 which showed relatively high probability to act on CYP 1A2 with value 0.84.

CHAPTER ONE

INTRODUCTION

1.1 Statement of the Problem

Influenza, according to WHO (World Health Organization), spreads around the world in seasonal epidemics, resulting the death between 250,000 and 500,000 people every year (Knobler et al., 2005). The three influenza pandemics that occurred in the 20th century and killed tens of millions people were Spanish flu in 1918, Asian flu in 1957, and then followed by Hong Kong flu in 1968-69. In the 21st century, the emergence of a highly pathogenic avian influenza virus of type A (H5N1) or bird flu, the pandemic of 2009 H1N1 (Swine flu), and also a recent case of a new avian influenza A (H7N9), which was firstly reported in China in March 2013, have led this disease becoming a threatening health issue in human (Hu et al., 2014).

Centers for Disease Control and Prevention (CDC) study of the disease burden of 2009 H1N1 pandemic, showed that the largest death burden took place in the African and Southeast Asian regions, with more than half of 2009 H1N1-related deaths occurred (Dawood et al., 2012). Since the first reported case in May 2009, Malaysia has witnessed 2,253 cases of H1N1 infection as of August 2009. The number of cases had been increasing and as of September 2009, there have been 73 death reported (Kementerian Kesihatan Malaysia, 2011).

Vaccination has become a primary strategy for the prevention of influenza. However in 2005, in some cases vaccination were inadequate, especially during the

course of pandemic. Current vaccine production methods cannot be carried out with the speed required to halt the development of new strains of influenza virus; therefore, it is possible that vaccine may not be available for the first wave of the virus outbreak. The limitations of vaccine efficacy, design and delay in strain specific vaccine production have stimulated the search for antivirals. Thus, antiviral agents form an important part of a rational approach to overcome epidemic influenza (Moscona, 2005, Boltz et al., 2010). Two classes of antivirals are currently approved for both prophylaxis and therapeutic treatment of influenza virus infection: M2-ion channel inhibitors (the adamantanes, amantadine and its derivative, rimantadine) and neuraminidase inhibitors (zanamivir and oseltamivir). Neuraminidase inhibitors have better tolerance, broader antiviral spectrum, and less potential for the emergence of resistance compared to the M2 inhibitor (Gubareva et al., 2000). Neuraminidase inhibitors are also currently the preferred treatment option for flu virus infection since they are less toxic and more effective (Beigel and Bray, 2008). Zanamivir and oseltamivir are examples of neuraminidase inhibitors, which are already licensed and commercially available for the treatment and prophylaxis of influenza. However, the poor oral bioavailability of zanamivir requires this drug to be administered by inhalation, while oseltamivir-resistant H1N1 viruses have emerged due to the latter broad use as oral medication. Recently, laninamivir, a potent neuraminidase inhibitor has been approved for use in Japan. Unfortunately, its effectiveness against oseltamivir-resistant neuraminidase in adults has not been proven, thus more study is needed to find new and more effective anti-influenza agents (Ives et al., 2002, Vavricka et al., 2011).

Currently, the activity of neuraminidase inhibitor is determined using a fluorogenic assay utilizing 2'-(4-Methylumbelliferyl)- α -D-N-acetylneuraminic acid

(MUNANA) as substrate. This method is quite sensitive and has been the most widely used and accepted method for detecting neuraminidase inhibition activity. However, typically in screening large libraries of chemicals, this assay is not very economical. A lot of enzymes are needed to conduct the experiments. Thus, fast, robust, sensitive, and reliable assays are needed. Therefore, the ultimate aim of this research is to develop an alternative neuraminidase inhibition assay, as well as to test this assay, to validate the inhibition of potential neuraminidase inhibitor from NCI database.

The present study focused on the development of neuraminidase inhibition assay using AlphaScreen™ technology to screen potential neuraminidase inhibitors. Following the optimization of the assay, it was intended that the assay was to be validated by testing known inhibitors for their inhibition. Since the assay is high throughput, molecular docking and virtual screening of compounds from National Cancer Institute (NCI) Diversity Set II database were also employed to obtain top *in silico* hits compounds for subsequent alpha screen inhibition assay. However, due to the failure of establishment of the assay, a traditional MUNANA *in vitro* assay was performed to investigate these compounds' inhibitory activities and their kinetic parameters. Finally the selected active compounds were studied for their pharmacokinetic properties *in silico* in an attempt to rationale their selection for further lead optimization, and possible drug development.

Specifically, the objectives of the study are to:

1. Virtually screen National Cancer Institute Diversity Set II compounds for potential neuraminidase inhibitors using molecular docking methods;
2. Screen these *in silico* hits compounds with *in vitro* fluorescence based assay with 2'-(4-Methylumbelliferyl)- α -D-N-acetylneuraminic acid (MUNANA) as substrate;
3. Determine V_{\max} , K_m for MUNANA substrate and K_i for the top compounds;
4. Predict the ADME properties of the top compounds screened with ACD/ADME Suite software.

1.2 The Influenza

1.2.1 Epidemics and Pandemics

Influenza is a serious infectious disease that affects respiratory tract and can lead to hospitalization and even death. Annual epidemic of influenza is estimated to be 3 to 5 million cases of severe illnesses and ~500,000 deaths globally. The high-risk groups of severe consequences and death include persons aged 65 years and above, children under 2 years, and persons with chronic medical conditions that put them at increased risk of developing influenza or its complications (Fauci, 2006, WHO, 2014).

Novel strains of Influenza A virus emerge sporadically every 1 to 2 years as influenza epidemics. The introduction of selected point mutations within hemagglutinin (HA) and neuraminidase (NA), the two surface glycoproteins of influenza virus, evade the human host defenses and therefore resulting in no lasting immunity against the virus, neither after natural infection nor vaccination. The small

changes of antigenicity of influenza virus are termed antigenic drift and become the basis for regular occurrence of the epidemic of influenza (Holmes et al., 2005).

On the other hand, influenza pandemics which involve a major change in the antigenicity of influenza A virus occur once every 10 to 50 years. At least three influenza pandemics have been recorded during the twentieth century: the Spanish flu in 1918-19, Asian Flu in 1957 and Hong Kong Flu in 1968 with mortality impact ranged from devastating to mild (Holmes et al., 2005, Lazzari and Stöhr, 2004, Oxford, 2000, Simonson, 2004). These viruses acquire a new subtype by re-assortment of RNA segments from different influenza viral strains. This genetic change, called antigenic shift, allows a viral strain to jump from one species of animal to another, including from animals to human (Figure 1.1) (Holmes et al., 2005, Wit and Fouchier, 2008).

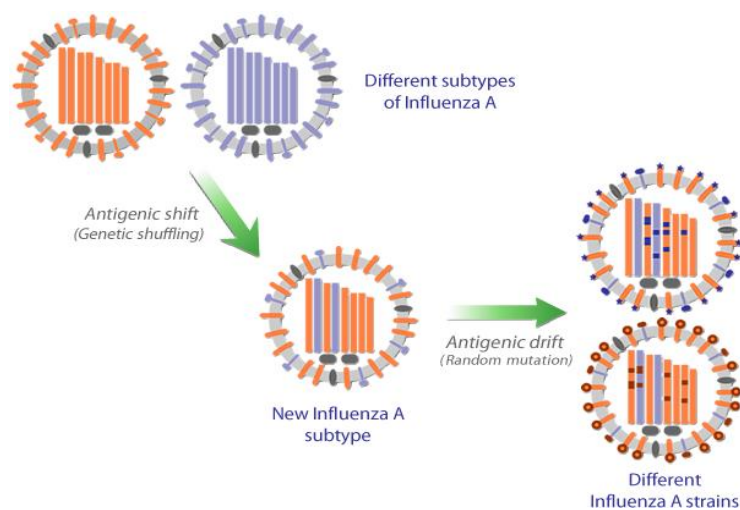


Figure 1.1 Influenza virus can change in two different ways. Antigenic drift is small changes in the virus that produces new virus strains. This may not be recognized by the body's immune system while antigenic shift is an abrupt, major change resulting new hemagglutinin and/or new hemagglutinin and neuraminidase proteins in influenza viruses.

The 1918 influenza pandemic, also referred to as Spanish Flu, was the first and the most devastating influenza pandemic in the 20th century. The pandemic spread globally by infecting 25-30% of the world's population and killing more than 50 million people (Taubenberger and Morens, 2006). Analysis of 1918 flu survivors suggested that 1918 pandemic was caused by H1N1-subtype influenza virus that contained genes derived from avian-like virus, which was also believed as the common ancestor of almost all influenza A cases, including re-assorted H3N2 and H2N2 viruses and drifted H1N1 viruses (Taubenberger et al., 2000, Taubenberger and Morens, 2006). These virus strains continued to circulate until they were replaced by H2N2 in 1957 influenza pandemic (Basler and Aguilar, 2008, Taubenberger and Morens, 2006). The influenza A virus with H2 subtype emerged in February 1957 in Hunan Province of China, considered clinically milder than 1918 pandemic virus with global mortality rate at 1-2 million deaths. The H2N2 virus circulated worldwide until H3N2 virus appeared in 1968 and replaced it. The 1968 influenza pandemic, also known as Hong Kong flu, was comparatively a milder pandemic with the death toll associated with it has been estimated around 1 million deaths (Oxford, 2000, Subbarao and Katz, 2000). The first influenza pandemic in 21st century began in 2009 when a new swine-origin influenza virus emerged and replaced the previous seasonal influenza H1N1. First identified in Mexico, the virus had spread to over 43 countries (Guarnaccia et al., 2013). The virus, often called "2009 H1N1", has been circulating in human and caused the first influenza pandemic in more than 40 years (CDC, 2014). Influenza A virus subtype H5N1, also called avian influenza or bird flu, is known to be highly pathogenic avian influenza A virus which caused devastating outbreaks in domestic poultry and give rise to the threat of human influenza pandemics. In July 2013 the WHO announced

630 confirmed human cases for avian influenza A (H5N1) in total which resulted in the deaths of 375 people since 2003 (WHO, 2013).

1.2.2 The Influenza Virus

Influenza virus is an enveloped virus which belongs to the family of Orthomyxoviridae with negative-sense, single stranded, and segmented RNA genome. The virus is classified into three serologically different types, influenza virus A, B, and C, with type A is the most virulence which cause severe and even fatal respiratory disease, influenza epidemic and also worldwide pandemic (Itzstein and Thomson, 2009, Gong et al., 2007, Nicholls et al., 2007, Samji, 2009). The influenza A viruses have eight segments which encode 11 viral genes: hemagglutinin (HA), neuraminidase (NA), matrix proteins M1 and M2, nucleoprotein (NP), non-structural (NS) proteins NS1 and NS2, polymerase acidic protein (PA), polymerase basic (PB) proteins PB1, PB2, and PB1-F2 (Samji, 2009). Influenza A viruses are further sub-divided based on the antigenic properties of their surface glycoproteins, HA and NA (Itzstein and Thomson, 2009, Gong et al., 2007). There are 18 known hemagglutinin subtypes and 11 known neuraminidase subtypes (CDC, 2014, Tong et al., 2013). A simple diagram of influenza A virus is shown on Figure 1.2. Hemagglutinin is the major surface protein of influenza A virus which consists of three identical subunits (homotrimeric) anchored to the lipid membrane of the virus. It is responsible for the initial contact between the virus and the target cell which contains terminal N-acetylneuraminic acid (sialic acid) residues. Moreover, hemagglutinin also contributes to the internalisation of the virus through fusion of the viral envelope with the target cell (Itzstein and Thomson, 2009). Influenza virus neuraminidase is a tetrametric protein and acts as glycohydrolase which removes N-acetylneuraminic acid (sialic acid) residues from

glycoconjugates in the surface of target cells, a crucial role in facilitating the release of newly synthesized virus from the host cells (Itzstein and Thomson, 2009, Xu et al., 2008).

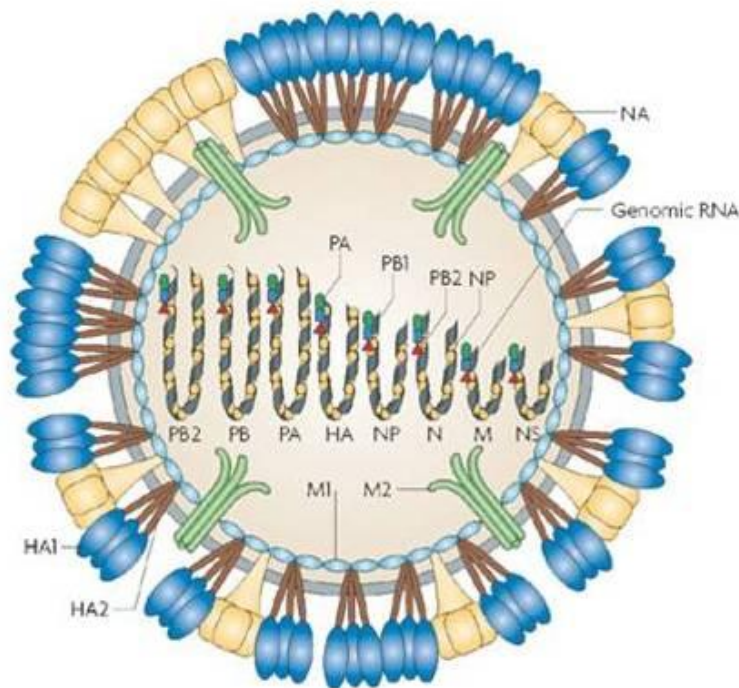


Figure 1.2 Diagram of influenza A virus. On the outside virus particles, 3 viral proteins: haemagglutinin (HA, trimers), neuraminidase (NA) (tetramers) and M2 (tetramers that make up ion-channels) are exposed (Hedestam et al., 2008).

1.2.3 Influenza Virus Life Cycle

The life cycle of influenza virus can be divided into several stages: virus entry to the host cell; entry of vRNPs into the nucleus; transcription and replication of the viral genome; export of vRNPs from the nucleus; then assembly and budding at the host cell plasma membrane. The first stage of virus infection is the binding of HA to sialic acid found in the surface of host cell's membrane. Sialic acids are bound to

carbohydrates of the membrane's glycoprotein with glycosidic linkage. There are two major linkages that are important for the specificity of HA, α (2, 3) linkage which is recognized by viral HA from avians and equines, whereas those from human recognize α (2, 6) linkage and those from swine recognize both. Upon binding with sialic acids, receptor-mediated endocytosis occurs and the virus enters the host cell in an endosome. The low pH of endosome (around 5 to 6) triggers the fusion of the viral and endosomal membrane. The acidic endosomes also open up the M2 ion channel and acidifies the viral core. This acidic environment in the virion allows vRNP to be released from M1 so that it is free to enter the host cell's cytoplasm as well as the nucleus. The viral proteins that make up the vRNP (NP, PA, PB1 and PB2) have recognized the nuclear localization signals (NLSs) which can bind to the cellular nuclear import machinery and thus, enter the nucleus to undergo transcription and replication. In order to be transcribed, the negative-sense RNA genome is first converted into a positive sense RNA as a template for the production of viral RNAs. The viral RNA dependent RNA polymerase (RdRp) initiates the synthesis of RNA internally in viral RNA, continued by cellular RNA Polymerase II (Pol II) that binds to DNA and starts transcription. vRNPs is then exported out from the nucleus through the nuclear pores. Before leaving the cell, virus needs to form viral particles. Therefore, the viral proteins that normally found within the viral lipid bilayer, i.e HA, NA, and M2, must be present and transported to the apical plasma membrane, since the virus particles bud from the apical side of polarized cells. After viral particles are formed, the sialic acid residues from glycoproteins and glycolipids are cleaved by neuraminidase, thus enable the viral particles to be released from the plasma membrane and goes on to infect neighboring cells (Samji, 2009). The virus life cycle is presented in Figure 1.3.

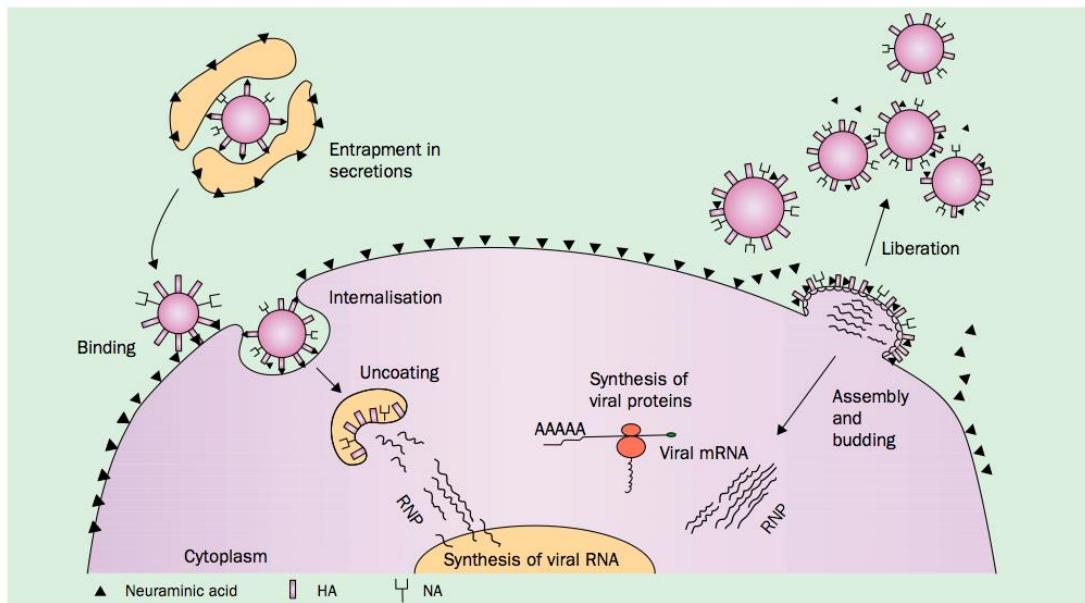


Figure 1.3 Influenza virus replication cycle (Gubareva et al., 2000).

1.2.4 Influenza Virus Neuraminidase

1.2.4.1 Structure of Neuraminidase

Influenza virus neuraminidase (EC 3.2.1.18) is a tetramer with four identical polypeptides composed of a cytoplasmic tail, a transmembrane domain, a globular head, and a stalk region (Gubareva et al., 2000, Gong et al., 2007). It destroys the receptors recognized by hemagglutinin by catalyzing the cleavage of terminal α -(2,3 or 2,6)-ketosidically linked sialic acid (N-acetylneuraminic acid) from a wide range of glycoconjugates, including glycoproteins and glycolipids, thus playing an important role in the life cycle of the virus (Gubareva et al., 2000, Itzstein and Thomson, 2009). Neuraminidase acts as a biological scissor that cut sialic acids residues both from upper respiratory tract mucins facilitating the movement of the virus, and also from the surface of glycoprotein of the newly synthesized virions, thus enabling the virus to be released from the host cell and continue to infect other cells (Itzstein and Thomson,

2009). The first X-ray crystal structure of neuraminidase was published in 1983. In 1992, Varghese and colleagues elucidated the structure of N2 subtype of neuraminidase at 2.9° Å resolutions as shown in Figure 1.4. The structure showed a tetrameric association of identical monomers with β -sheet propeller (Gong et al., 2007, Varghese et al., 1992).

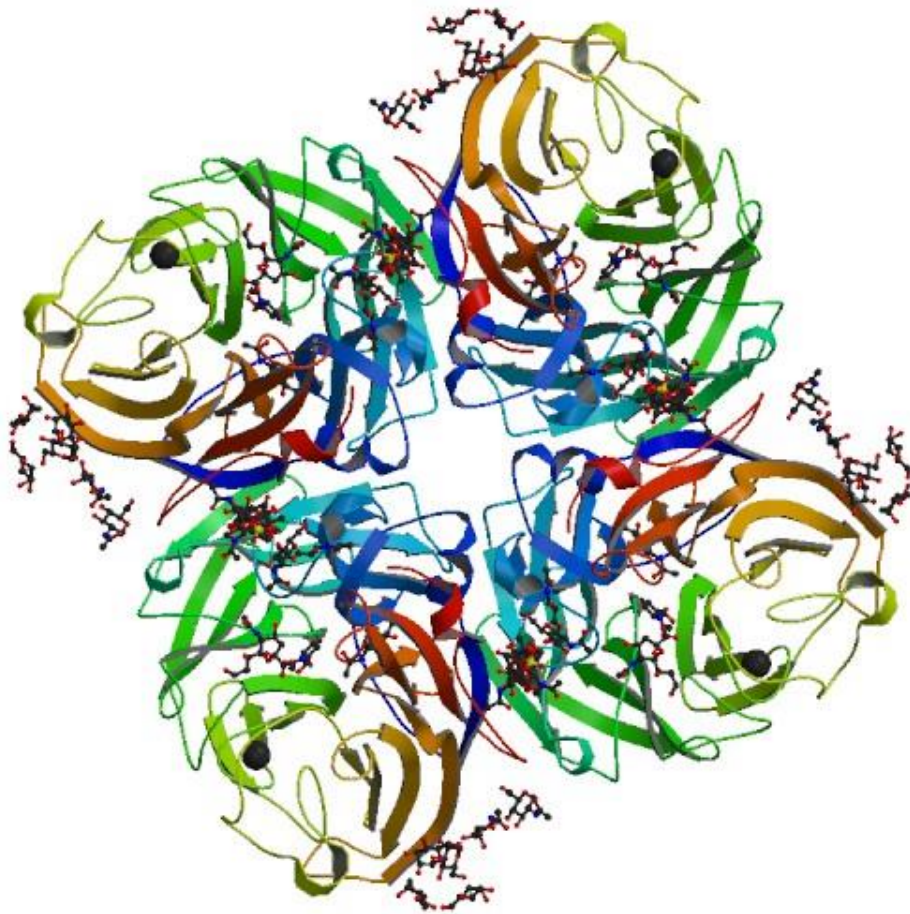


Figure 1.4 Three dimensional structure of an N2 neuraminidase tetramer in complex with sialic acids (PDB entry 2BAT) (Varghese et al., 1992).

The structural studies on NA enzymes from four influenza A viruses and two influenza B virus subtypes have discovered that NA structure is well conserved. Investigation conducted by Gong and colleagues on several NA structures showed that they have a generally similar topology to N2 NA (Gong et al., 2007).

1.2.4.2 The Substrate and the Active Site of Neuraminidase

Sialic acid (SA) is a generic term for nine-carbon sugar acids that are widely expressed on the surface of all cells in all animals of the deuterostome lineage (vertebrates and so-called "higher" invertebrates) and also in certain pathogenic or symbiotic bacteria that associate with them. It features conspicuously at terminal positions of the surface-exposed glycoconjugates (Severi et al., 2007, Suzuki et al., 2000, Varki and Gagneux, 2012).

Sialic acid was first discovered about 70 years ago as a major product released by mild acid hydrolysis of brain glycolipids or salivary mucins by Gunnar Blix, Ernst Klenk, and other scientists (Du et al., 2009). Erwin Chargaff's group then found out that "receptor-destroying enzyme" of influenza viruses was able to release sialic acid from macromolecules and thus, acts as sialidase (Varki and Schauer, 2009). Karl Meyer's group observed a similar activity in bacteria, then the name "neuraminidase" was suggested for this activity by Alfred Gottschalk in 1957. Partially because of its discovery in salivary mucins (Greek: sialos), this family was named the "sialic acids" (Varki and Schauer, 2009).

Sialic acids rarely occur freely in nature. They are more commonly found as components of oligosaccharide chains of mucins, glycoproteins, and glycolipids. They usually occupy terminal, non-reducing positions of oligosaccharide chains of complex carbohydrates on outer and inner membrane surfaces in various linkages, mainly to galactose, N-acetylgalactosamine, and other sialic acid moieties, where they are highly exposed and functionally important. Sialic acids consist of a family of 43 naturally occurring derivatives of the nine-carbon sugar neuraminic acid (5-amino-3, 5-dideoxy-

D-glycero-D-galactononulsonic acid). One branch of the sialic acid family is N-acetylated to form N-acetylneuraminic acids (Neu5Ac, NANA, Sia), which are the most widespread form of sialic acid and almost the only form found in human. The other branch is based on N-glycolylneuraminic acids (Neu5Gc) where the amino group is substituted with N-glycolyl group. These are found commonly in many animal species (best investigated in porcine tissues), but not found in humans except in the case of a particular cancer (Suzuki et al., 2000, Wang and Brand-Miller, 2003). Two most common forms of sialic acid are *N*-acetyl neuraminic acid (Neu5Ac) and *N*-glycolylneuraminic acid (Neu5Gc) as shown in Figure 1.5.

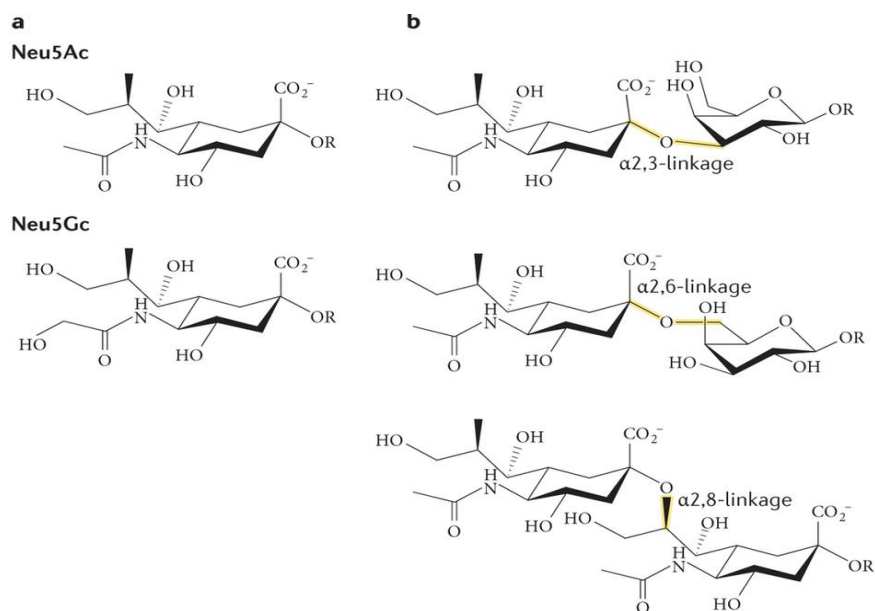


Figure 1.5 **a.** The two most common sialic acids are *N*-acetyl neuraminic acid (Neu5Ac) and *N*-glycolylneuraminic acid (Neu5Gc). **b.** Sialic acids are attached to carbohydrate chains on glycoproteins and glycolipids via different glycosidic linkages. The most common linkage types are $\alpha 2, 3$ -linkage to a galactose residue, $\alpha 2,6$ -linkage to a galactose moiety or to an *N*-acetylgalactosamine moiety, and $\alpha 2,8$ -linkage to another sialic acid moiety on a glycan (Stencel-Baerenwald et al., 2014).

Neuraminidase is an exo-glycoside hydrolase that hydrolyzes terminal sialic acid residues from any glycoconjugate, including viral glycoprotein. In general, glycoside hydrolases (GH) are a group of enzyme which catalyze the hydrolysis of the glycosidic bond between two or more carbohydrates or between carbohydrates and

non-carbohydrates moiety. This group is classified in families based on amino acid sequence similarities. As of July 2015, CAZy (Carbohydrates-Active Enzyme) database describes the present knowledge of 133 glycoside hydrolase families. Neuraminidase, either from bacteria or viruses, belong to glycoside hydrolase family 33, 34, 83 (Cantarel et al., 2009, Lombard et al., 2014). Hydrolysis of neuraminidase substrate was solvent-mediated and involved a sialosyl cation transition state intermediate. The pathway of neuraminidase consists of four major steps. The first step is the binding stage where the carboxylate group transforms from the axial position into a pseudo-equatorial position due to the charge-charge interactions to Arg 118, Arg292, and Arg371 and steric constraints with residue at the base of the active site, such as Tyr406. The following step involves proton donation from solvent and formation of the endocyclic sialocyl cation transition-state intermediate. The hydrogen bonding network of water molecules and protein residues leading from a charged group on the protein surface to water molecules could facilitate proton donation. Asp 151 and Arg 152, and to a certain extent, for Glu 227, are believed to contribute to the stability of the cationic intermediate. The active site of neuraminidase with its important residues is presented in Figure 1.6. The final two steps are the formation and release of Neu5Ac. The expulsion of the product from the active site is favored by the mutarotation of the initial β -anomer to the more thermodynamically stable α -anomer for Neu5Ac in solution as shown in Scheme 1.1 (Gong et al., 2007).

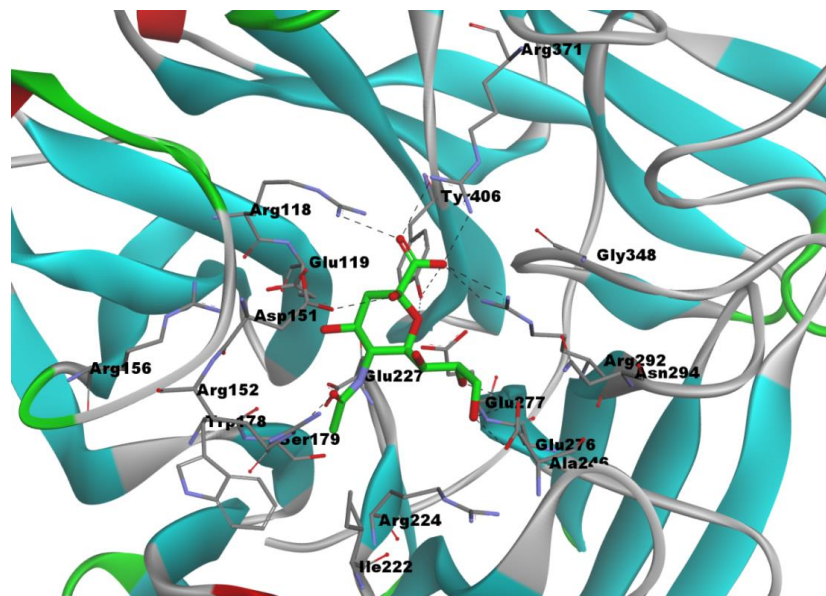
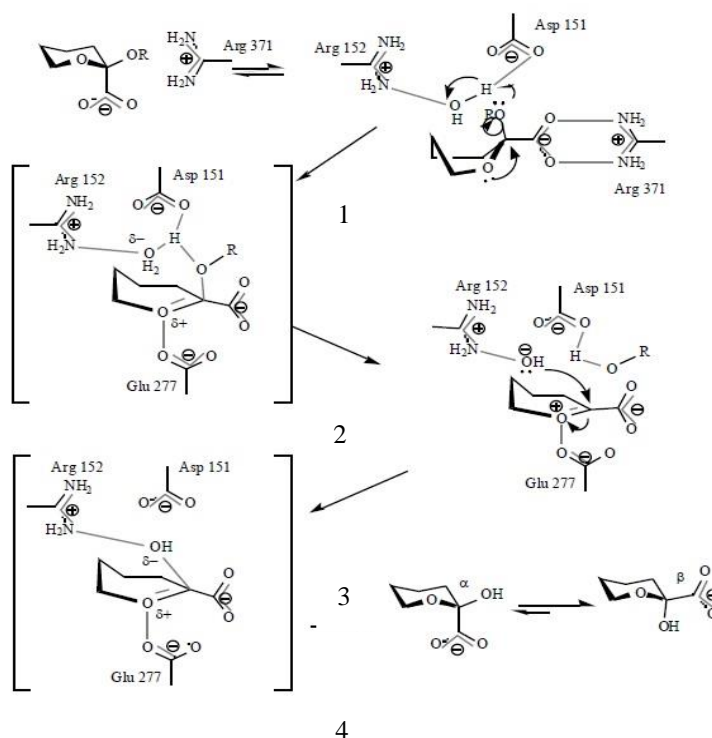


Figure 1.6 Neuraminidase active site consists of functional amino acid residues Arg118, Asp151, Arg152, Arg224, Glu 276, Arg292, Arg371, and Tyr406, which are in direct contact with sialic acid, and structural amino acids residue Glu119, Arg156, Trp178, Ser179, Asp (or Asn in N7 and N9)198, Ile222, Glu227, Glu277, Asp293, and Glu42 (Protein Data Bank ID: 2BAT www.rcsb.org) (Varghese et al., 1992) .



Scheme 1.1 Reaction steps and corresponding intermediates of catalytic pathway of neuraminidase (Gong et al., 2007).

1.2.4.3 Neuraminidase Inhibitor

The importance role of neuraminidase in the life cycle of influenza virus as well as the conserved nature of the neuraminidase active site among influenza viral strains have resulted the enzyme to be considered as an excellent target for antiviral drug design. Several approaches have led to the discovery of neuraminidase inhibitors through random screening or development and modifications of the functional groups of original substrate (Itzstein and Thomson, 2009).

Neuraminidase cleaves sialic acid residues on the host cell receptor to which the newly formed virion attached, enabling the virus to be released and invade the new host cells and continue the infections. Neuraminidase inhibitors mimic the natural substrate of neuraminidase and bind to the active site. It works by blocking the activity of viral neuraminidase preventing the enzyme from cleaving the cell receptors. Without the activity of neuraminidase, virus infection would be limited to only one round of replication, rarely enough to cause disease (Moscona, 2009).

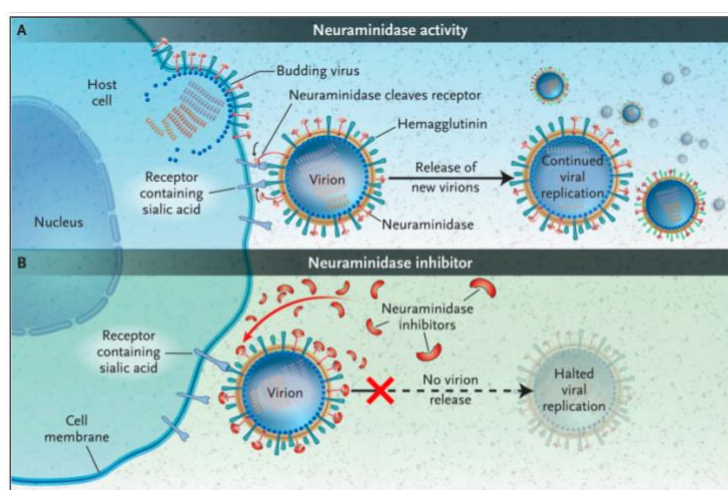


Figure 1.7 Mechanism of Action of Neuraminidase Inhibitors. Panel A shows the action of neuraminidase in the continued replication of virions in influenza infection. The replication is blocked by neuraminidase inhibitors (Panel B), which prevent them from being released from the surface of infected cells (Moscona, 2005).

The ability of transition-state analogues of sialic acids in inhibiting the activity of influenza neuraminidase was first discovered in 1970s (Air, 2012), and the design of highly effective inhibitors became feasible when analysis of three dimensional structure of influenza neuraminidase disclosed the location and structure of catalytic site (Moscona, 2009). Neuraminidase inhibitors, zanamivir (Relenza) and oseltamivir (Tamiflu) have been approved by the US FDA in 1999 as antiviral drugs for influenza treatment and prophylaxis (Boltz et al., 2010, Moscona, 2009). Zanamivir mimics the natural substrate closely, fits into the active site's pocket of neuraminidase and interacts with the protein in the most favorable way. Zanamivir is administered by oral inhalation which delivers the drug to the respiratory tract directly, while oseltamivir was developed through modifications to the sialic acids analogue framework (including the addition of lipophilic side chain) which allow the drug to be used orally (Moscona, 2009). Neuraminidase crystal structure in complex with zanamivir reveals the active site of neuraminidase with its important residues and their interaction with zanamivir (Figure 1.8). Asp151 is hydrogen bonded via one of the carboxyl oxygens to the secondary guanidinyll nitrogen of zanamivir, and the main-chain carbonyl oxygen interacts with one of the guanidino NH₂ groups of the inhibitor. Arg152 also forms hydrogen bond with the carbonyl oxygen of the N-acetyl group of zanamivir. Val149 undergoes a Ctranslation of about 7.0 Å, as observed in the recent H5N1 NA structure. The side chain of Glu119 also adopts a different orientation, to point away from Glu227, interacting with Arg156 instead to accommodate the 4-guanidino group of zanamivir. Other conserved interactions among all other NAs include that of the carboxyl group of zanamivir with three conserved arginine residues, Arg118, Arg292, and Arg371, and that of the two terminal hydroxyl groups on the glycerol side chain on the C-6 position with the carboxylate of Glu276 (Xu et al., 2008).

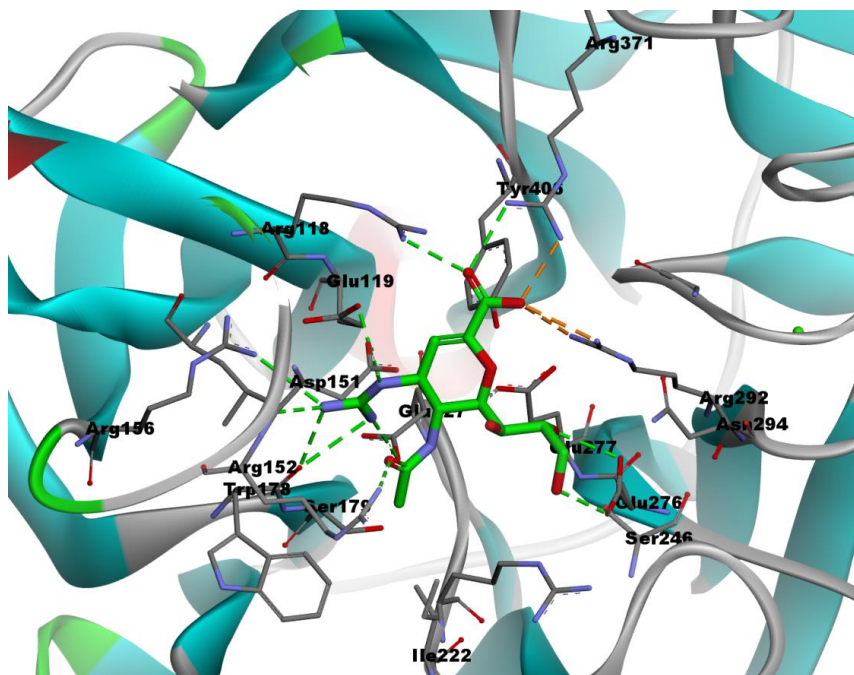


Figure 1.8 Neuraminidase crystal structure in complex with zanamivir (PDB ID: 3B7E) (Xu et al., 2008).

1.3 Computational Methods for Drug Discovery

The advanced technologies in the field of molecular biology, such as high-throughput protein purification, crystallography and nuclear magnetic resonance spectroscopy techniques have contributed greatly to the increase of structural data of proteins and protein-ligand complexes (Meng et al., 2011). These structural discovery also allow the computational methodologies to become a crucial components for drug discovery and development strategies, from hit identification to lead optimization, and approaches such as ligand- or structure based virtual screening techniques (Kitchen et al., 2004). Compared with traditional experimental high-throughput screening (HTS) which has been applied to generate and screen large compound libraries, virtual screening is a more direct and rational drug discovery approach and has the advantage

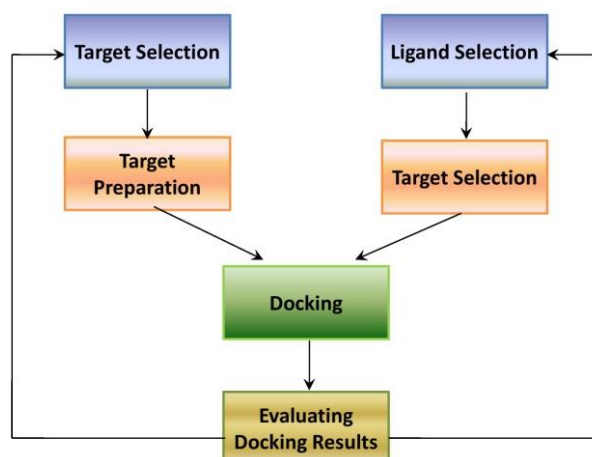
of faster, more economical and effective screening (Moitessier et al., 2008, Meng et al., 2011).

Virtual screening can be classified into ligand-based and structure-based method. Ligand-based methods, such as pharmacophore modelling and quantitative structure activity relationship (QSAR) methods, can be employed when a set of active ligand molecules is known and no or little structural information is available for targets. As to structure-based drug design, molecular docking is the most common method which has been widely used ever since the early 1980s (Meng et al., 2011). It remains a field of vigorous research, having become a useful tool in drug discovery efforts, and primary component in many drug discovery program (Sousa et al., 2006). Molecular docking, which is usually performed between a small molecule and a target macromolecule, is often referred to as ligand-protein docking. This method allows us to characterize the behaviour of small molecules (ligands) in the binding site of a target (protein, DNA, or RNA macromolecules) as well as to elucidate fundamental biochemical processes, to predict molecular recognition, both structurally, finding likely binding modes, and to predict binding affinity (Morris and Lim-Wilby, 2008, Meng et al., 2011). Molecular docking has a wide variety of uses and applications in drug discovery, including structure–activity studies, lead optimization, finding potential leads by virtual screening, providing binding hypotheses to facilitate predictions for mutagenesis studies, assisting x-ray crystallography in the fitting of substrates and inhibitors to electron density, chemical mechanism studies, and combinatorial library design. Virtual screening on the basis of molecular descriptors and physicochemical properties of (in)active ligands has great usefulness in finding hits and leads through library enrichment for screening (Morris and Lim-Wilby, 2008, Pozzan, 2006).

The docking process involved two basic steps: prediction of the ligand conformation as well as its position and orientation within the site and assessment of binding affinity. Docking can be achieved through two interrelated steps; first by sampling conformations of the ligand in the active site of the protein; then ranking these conformations via a scoring function and thus give the prediction of the ligand-receptor complex structure (Meng et al., 2011). There are various docking programs, such as AutoDock, DOCK, GOLD, ZDOCK, M-ZDOCK, MS DOCK, FLEXX, Surflex, MCDOCK, and others, based on specific search algorithm (Dias and de Azevedo Jr, 2008).

AutoDock is one of the most popular docking programs developed to provide an automated procedure for predicting the interaction of ligand with biomolecular targets (Morris et al., 2002, Sousa et al., 2006). All docking methods require a scoring function to rank the various candidate binding modes, and a search method to explore the state variables. Scoring functions can be empirical, force field based, or knowledge based, whereas search methods fall into two major categories: systematic and stochastic. Systematic search methods sample the search space at predefined intervals, and are deterministic. Stochastic search methods iteratively make random changes to the state variables until a user-defined termination criterion is met, so the outcome of the search varies. Search methods can also be classified by how broadly they explore the search space, as either local or global. Local search methods tend to find the nearest or local minimum energy to the current conformation, whereas global methods search for the best or global minimum energy within the defined search space. Hybrid global–local search methods have been shown to perform even better than global methods alone, being more efficient and able to find lower energies. In AutoDock 4, for example, there are choices of two local search methods (Solis and Wets and Pattern

Search); two global search methods: Monte Carlo (MC) simulated annealing (SA) and the genetic algorithm (GA); and one hybrid global–local search method, the Lamarckian GA (LGA) (Morris and Lim-Wilby, 2008, Sousa et al., 2006).



Scheme 1.2 Typical docking workflow. This flowchart shows the key steps common to all docking protocols. The 3D structures for the target macromolecule and the small molecule must first be chosen, and then each structure must be prepared in accordance with the requirements of the docking method being used. Following the docking, the results must be analyzed, selecting the binding modes with the best scores (Morris and Lim-Wilby, 2008).

AutoDock 4.2 uses a semi empirical free energy force field to evaluate conformation during docking simulations. The force field was parameterized using a large number of protein-inhibitor complexes for which both structure and inhibition constant, or K_i are known.

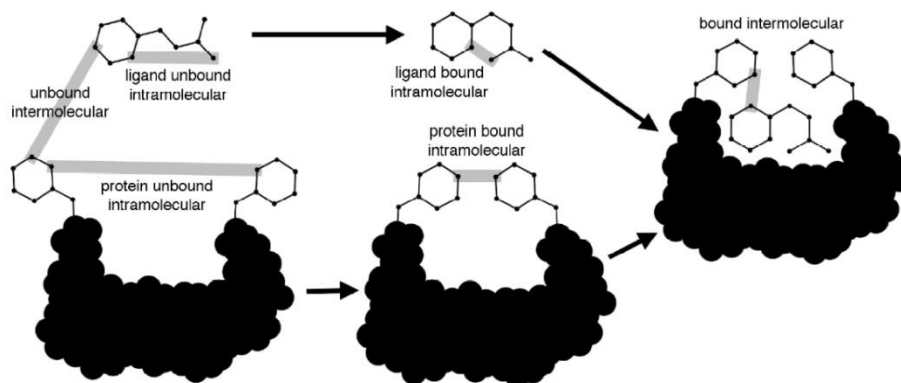


Figure 1.9 Mechanism of ligand interactions in the receptor binding site (Morris et al., 2010)

The force field evaluates the binding in two steps. The ligand and protein start in an unbound conformation. In the first step, the intramolecular energetics are estimated for the transition from these unbound states to the conformation of the ligand and protein in the bound state. The second step then evaluates the intermolecular energetics of combining the ligand and protein in their bound conformation (Figure 1.9). The force field includes six pair-wise evaluation (V) and an estimate of the conformational entropy lost upon binding (ΔS_{conf}):

$$\Delta G = (V_{bound}^{L-L} - V_{unbound}^{L-L}) + (V_{bound}^{P-P} - V_{unbound}^{P-P}) + (V_{bound}^{P-L} - V_{unbound}^{P-L} + \Delta S_{conf})$$

Equation 1

where L refers to the ‘ligand’ and P refers to the ‘protein’ in a ligand-protein docking calculation. Each of the pair-wise energetic terms includes evaluations for dispersion/repulsion, hydrogen bonding, electrostatics, and desolvation:

$$V = W_{vdw} \sum_{i,j} \left(\frac{A_{ij}}{r_{ij}^{12}} - \frac{B_{ij}}{r_{ij}^6} \right) + W_{hbond} \sum_{i,j} E(t) \left(\frac{C_{ij}}{r_{ij}^{12}} - \frac{D_{ij}}{r_{ij}^{10}} \right) + W_{elec} \sum_{i,j} \frac{q_i q_j}{\epsilon(r_{ij}) r_{ij}} + W_{sol} \sum_{i,j} (S_i V_j + S_j V_i) e^{(-r_{ij}^2 / 2\sigma^2)}$$

Equation 2

(Morris et al., 2010)

Autodock is distributed with a GUI called AutodockTools (ADT; <http://mgltools.scripps.edu>). ADT is a part of MGLTools and built on the Python Molecular Viewer (PMV), it helps to prepare the ligand and receptor input files, and to set up the Autogrid and Autodock calculations. The key stages in docking are: 1) target selection and preparation, 2) ligand selection and preparation, 3) docking setup, and 4) evaluating docking results (Morris and Lim-Wilby, 2008).

1.4 Enzyme Kinetics

1.4.1 Maximum Velocity (V_{max}) and Michaelis-Menten Constant (K_m)

In vitro characterization of enzyme studies and substrate metabolism involves determination of qualitative profiles and quantitative parameters. Quantitative parameters generally include the estimation of kinetic parameters, such as maximum velocity (V_{max}) and Michaelis-Menten constant (K_m). Enzyme inhibition studies are conducted to characterize the type of inhibition process (i.e., competitive, uncompetitive, or noncompetitive) and to determine the inhibition constant (K_i) (Kakkar et al., 1999).

Kinetic study explains the rate of reaction, how fast an enzyme converts substrate to form product, which is also known as velocity. To determine velocity,

product (or substrate) concentration and time have to be measured. Velocity is the slope of a plot of product (or substrate) concentration against time (Figure 1.12) (Gilbert, 2000).

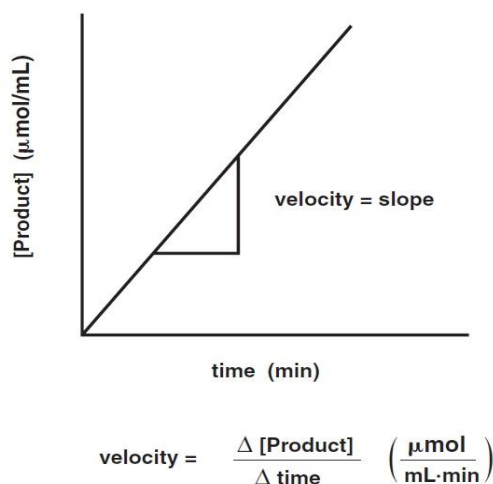
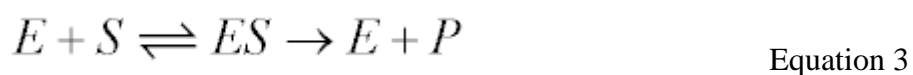


Figure 1.10 Velocity of product formation or substrate disappearance is defined as the change in product concentration per unit time. Velocity is the slope of a plot of product concentration against time (Gilbert, 2000).

The Michaelis-Menten constant, K_m , can be described as the equilibrium constant of the reversible combination of an enzyme with its substrate. It takes the state where a substrate S binds reversibly to an enzyme E to form an enzyme-substrate complex ES , which reacts irreversibly to generate a product P and also regenerates free enzyme E . This system can be represented as follows:



The Michaelis-Menten equation for this system is:

$$v = \frac{V_{\max}[S]}{(K_m + [S])} \quad \text{Equation 4}$$